International Journal of Pattern Recognition
and Artificial Intelligence
Vol. XX, No. X (2006) 1–18

World Scientific
www.worldscientific.com

SSDC-GAN: Same Size Densely Connected GAN for Dehazing Network

Juan Wang[1,2], Chang Ding[1,2], Minghu Wu[1,2,*], Guanhai Chen[1,2], Liquan Guo[1,2], Zishan Liu[1,2]
[1] *Hubei Energy Internet Engineering Technology Research Center, Hubei University of Technology Wuhan 430068, China*
[e-mail: d8425@foxmail.com]
[2] *Hubei Laboratory of Solar Energy Efficient Utilization and Energy Storage Operation Control, Hubei University of Technology, Wuhan 430068, China*

Haze weather has seriously affected the quality of external image collection, and needs to be solved urgently. Unfortunately, most existing deep learning models have trouble with the loss of detail and color deviation in the real-world hazy image after being dehazed, which hinders their application to practical projects, especially for high quality images require works. To address the problem, we propose a novel connected mode (SSDC) employed in end-to-end dehazing model that does not rely on the atmospheric scattering model and precise priors, but simplifies the image dehazing problem to a conversion problem between images. Generator of SSDC-GAN employs encoder-decoder and proposed same size densely connected architecture with residual blocks to maintain image feature information when processing. Meanwhile, a depth discriminator is utilized to balance the relationship between generator and discriminator during training. SSDC-GAN achieves the purpose of dehazing in the real-world hazy images and retains the accurate contour and color information. To test the dehazing effect of the model on real hazy image datasets, we abandoned the indoor and outdoor synthetic datasets in favor of real-world datasets O-HAZE and I-HAZE. Experimental results demonstrate that the proposed method performs favorably against the state-of-the-art dehazing approaches on various benchmarks.

Keywords: Image Dehazing; Densely Connected; Generative Adversarial Network (GAN).

1. Introduction

Haze weather appears as a phenomenon where the atmosphere covers the scene. A large number of suspended particles will make an impact on collected images such as reflection, refraction and absorption of atmospheric light. The phenomenon will reduce the scene visibility, lead to blurred image details, low contrast, color distortion, and information loss. Interfere with the follow-up work of extracting useful information and solving practical problems in computer vision and other works. Inevitably, the problem of how to improve image quality and reduce the interference of photoelectric acquisition equipment in harsh environments must be solved.

Atmospheric scattering model[1] is employed to describe the relationship between haze and non-haze images:

$$I(x) = J(x)t(x) + A(1 - t(x)) \tag{1}$$

Where the x denotes the pixel or image, $I(x)$ represents the observed intensity (haze image), $J(x)$ denotes scene radiance (clean image), and A denotes the global atmospheric

light that exist in air. A is variable but when it is regarded as homogeneous, the medium transmission $t(x)$ can be described as follows,

$$t(x) = e^{-\beta d(x)} \tag{2}$$

Where β denotes the scattering coefficient of the atmosphere, and $d(x)$ is the distance between object and vision sensor.

Dehazing algorithms can be the pre-processing for most of the computer vision tasks, for example, object detection[2][3], image classification[4] and semantic segmentation[5]. Most of the work employs surveillance cameras and other sensors to capture pedestrians and cars images, subsequently extracts visual labels, employs intelligent analysis technology to process and classify information that requires high-quality information. Whereas, collected hazy images reduce the accuracy and efficiency of works.

In this paper, image dehazing problem has been converted into image-to-image translation problem. To improve the quality of image generation and preserve most of the image details information, inspired by DCPDN connection mode[6], we propose a novel connection architecture employed in generator, GAN. Experiment (Fig. 1) shows our method has achieved excellent performance in preserving color information.

In case of model collapses during training, G (generator) with high-quality conquered D (discriminator) because of sophisticated structure optimization, we deepen the network layer of discriminator and reduce the step size of the convolution kernel.

(a)Hazy (b)DehazeNet[7] (c)AOD[8] (d)Our method (e)Ground Truth

Fig. 1. Color wheel dehazing effects via different methods.

Our main contributions can be summarized as follows.:

• We propose an end-to-end dehazing model with novel connection architecture in generator for retaining information of the images in SSDC-GAN. The same size densely connected method is considered from the perspective of image features, that greatly reduces network parameters, enhances image dehazing effects and alleviates the gradient vanishing problem.

• SSDC-GAN employs a generator which combines an encoder and decoder structure with embedded residual blocks in pre-trained Densenet-121 to better preserve the image details. We employ perceptual loss to generate more visually pleasing images. SSDC-GAN optimized a deep discriminator structure to deal with network complexity imbalance problem for non-haze images generation.

Several advanced dehazing algorithms, and the construction of the SSDC-GAN model, are discussed in the following sections. In Section 2, recent related dehazing methods are introduced, while the architecture of SSDC-GAN is illustrated in Section 3 and the experiment is detailed in Section 4. Finally, the conclusion and future research directions are provided in Section 5.

2. Related work

Numerous dehazing algorithms have been proposed, and algorithms have been categorized into traditional method, priori-based method and deep learning-based method, we make an analysis about it in detail.

2.1. *Traditional Image Dehazing*

Image dehazing work has attracted researchers' attention, the algorithm can be divided into two directions: image enhancement and image restoration. Dehazing methods based on image enhancement does not consider the reasons for image degradation. It improves the image quality and the clarity of image by enhancing the useful information in image while suppressing or removing the unwanted information. Those methods have several characteristics, such as project started early, relatively mature technology, and wide applicability. The typical hazy image enhancement methods mainly include histogram equalization algorithm[9], Retinex algorithm[10] and image fusion-based methods.

2.2. *Prior-based Dehazing*

The method based on prior knowledge refers to utilizing the characteristics of the parameters in the model as hypotheses to make the parameters solvable. Methods based on prior knowledge make the recovery method of single hazy image develop rapidly and has made breakthrough progress. The dark primary color (DCP) prior method[11] is a typical representative of haze image restoration method based on prior knowledge. He et al. takes the minimum value of the local area as a preliminary estimation of the superimposed ambient light. The non-haze image is restored through the edge optimization algorithm combined with the atmospheric scattering model directly. Based

on the fact that haze-free images possess a higher contrast than the hazy images, Tan et al. [12] increases the contrast of target images to obtain high-visibility images. CAP[13] shows a linear relationship between image depth, brightness and saturation. Those methods have demonstrated effective results at that period, but consumed plenty of time and memory, which limits application promotion. Design of these features requires experienced domain experts, and cannot be fully applied to the variable natural images.

2.3. *Learning-based Dehazing*

Hazy image restoration algorithm based on deep learning is obtained by automatic machine learning without manual design of feature extractors. DehazeNet employs a specially designed convolutional neural network to learn the features of hazy images and solve the difficulties of manual feature design. Taking multi-scale features of haze images into consideration, researchers proposed a multi-scale convolutional neural network to absorb the features of hazy images and estimate transmittance. Through deformed atmospheric scattering model, Li et al. proposed the All-in-One dehazing convolutional neural network, the innovation compared to the previous method is that AOD-Net is able to estimate the haze-free image directly.

DCPDN utilizes edge-preserving encoder with densely connected pyramids, and it was used to accurately estimate transmission mapping, EPDN[14] employed a three-part network consisting of generator, discriminator, and two enhancer blocks, they treated the dehazing task as an image-to-image translation problem.

Methods based on convolutional neural network[15][16][17] attract researchers' attention and achieved positive results on image dehazing works.

2.4. *Generative Adversarial Networks*

GAN has become one of the frequently utilized network architectures in recent years, and the network has been used in image generation[18], image denoise[19] and image derain[20]. Similarly, GAN is also employed in the dehazing by image conversion. Cycle-Dehaze[21] employs two paired generators and discriminators as the backbone network for dehazing, DehazeGAN[22] employs Densenet[23] to extract image features and generate visually realistic dehazed images. HardGAN[24] is utilized to process images with non-homogeneous haze, while, method can eliminate dense haze as well.

3. Proposed Method

We employ the GAN framework to convert the dehazing problem into a image conversion problem, and optimize the network architecture to retain features.

3.1. *Same Size Densely Connected Encoder-Decoder*

To preserve the image and color features information as possible by modifying the network structure without estimating intermediate parameters. Generator is required to retain the image content and cover as much detail as possible. Recently works have

revealed the dense connections possess the potentiality to promote feature extraction and utilization, especially for low-level vision tasks. For example, previous works[25][26] demonstrate the excellent ability of densely connected encoder-decoder in retaining image feature information, including the color and target outline details.

In addition to the commonly encoder and decoder connections, we propose a novel same size connection approach. SSDC perform different pooling operations on the output images in individually generator layer, including pooling layers with filters of sizes 2, 4, 8 and 16 to dwindle the feature map, and insert the reduced image into the network layer of the corresponding size.

SSDC-GAN employs the Denseblock and Transblock in pre-trained densenet-121 to extract image features in encoder, and make pooling operations with different filter sizes. At the end of each Denseblock & Transblock layer there are 2× times downscaling for feature map continues to shrink. In the process of gradually shrinking the feature map, the network extracts the output image of each layer and projects to the decoder layers of the corresponding size. At the same time, the network merges one or more pooling operations of the corresponding size layers and different filters.

SSDC-GAN sets feature map transmission as follows: $IM^{i}_{d,ln}$ denotes the input feature graph of the nth layer of the decoder, $OM^{i}_{e,ln}$ denotes the output feature map of the nth layer of the encoder, and the following formula demonstrates the input of the second layer in the decoder network:

$$IM^{i}_{d,l2} = IM^{i}_{e,l1} \big/ 16 + IM^{i}_{e,l2} \big/ 4 + IM^{i}_{e,l3} \big/ 2 + IM^{i}_{e,l4} + OM^{i}_{d,l1} \tag{3}$$

In the Eq. (3), the first three variables on the right equation are the input characteristic images of the first, second and third layers of the encoder for unequal pooling, and the output of the first layer in the decoder is attached. The input of the third layer in decoder is:

$$IM^{i}_{d,l3} = IM^{i}_{e,l1} \big/ 8 + IM^{i}_{e,l2} \big/ 2 + IM^{i}_{e,l3} + OM^{i}_{d,l2} \tag{4}$$

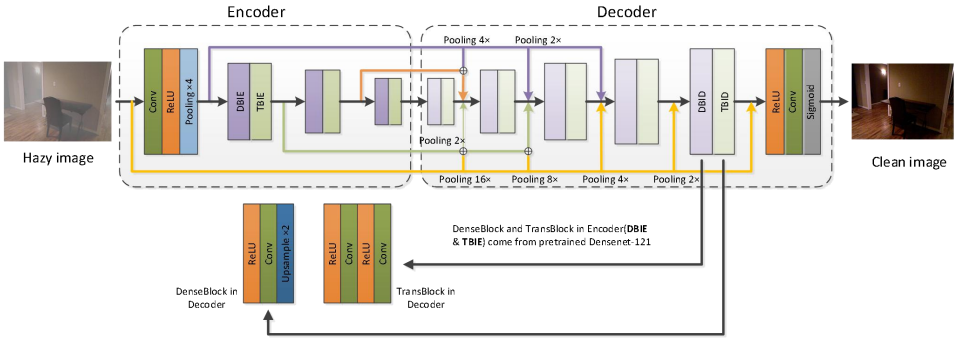

Fig. 2. Generator.

Input of the fourth layer of decoder is:

$$IM^{i}_{d,l4} = IM^{i}_{e,l1} \big/ 4 + IM^{i}_{e,l2} + OM^{i}_{d,l3} \tag{5}$$

The fifth layer input of decoder is:

$$IM_{d,l5}^{i} = IM_{e,l1}^{i} / 2 + OM_{d,l4}^{i} \tag{6}$$

The input of the sixth layer of decoder is:

$$IM_{d,l6}^{i} = IM_{e,l1}^{i} + OM_{d,l5}^{i} \tag{7}$$

As shown in Fig. 2, the encoder comprises three DenseBlocks & TransBlock (in Encoder) modules, and convolution layer + ReLU with pooling layer (filter size 4). In the decoder module, there are 5 DenseBlocks & TransBlock (in Decoder) modules utilized to upscale the feature maps and restore the resolution.

3.2. *Depth Discriminator*

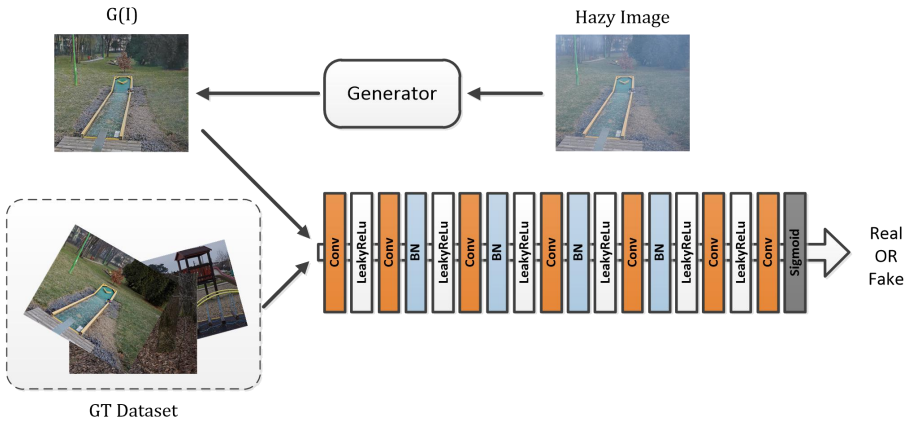

Fig. 3. Depth discriminator, by increasing the step size and layer depth.

To compare the capabilities of the original generator and SSDC-GAN generator, we first design a depth discriminator(Fig. 3) initially, whose deeper network layers structure supply the discriminator elaborate feature extraction, analysis and judgment ability, which means that the rival generator is required to possess the equally image generation ability. Compared to the original D, we deepen D and increase number of layers with the purpose of better image information collection generated by G (generator) and compare the image features of real datasets, so as to determine the image authenticity better and more accurately. D confronts the G to achieve Nash balance. To balance the overall network complexity, the stride of the convolution kernel has been increased to 2, which will greatly reduce the number of parameters for each layer, and increase processing efficiency.

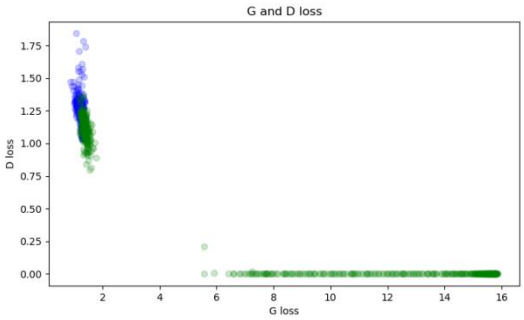

Fig. 4. The scatter diagram represents the loss distribution of G and D at the same time. Green points denote the original discriminator, and blue is the depth discriminator.

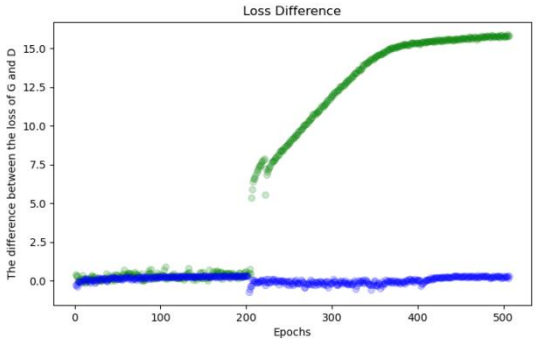

Fig. 5. The absolute value of loss difference between G and D varies with training times.

In the Fig. 4 and Fig. 5, we compare the original generator and the SSDC-generator. Fig. 4 demonstrates the loss difference distribution of generator and discriminator in GAN network under the condition of utilizing the original generator and the SSDC-G. Fig. 5 demonstrates the relationship between the absolute value of the loss difference between generator, discriminator, the training times in the original G network and the SSDC-G network respectively. Sampling is performed every 5 epochs during drawing, one epoch in figures is equal to 5 epochs in training.

As shown in Fig. 5, the problem of vanishing gradient occurred in the original generator at epoch 200, discriminator loss rapidly approached 0 in subsequent iterations, while generator loss increased and tended to be constant after epoch 400. The phenomenon demonstrates the strong image discrimination ability of depth discriminator overwhelms the image generation's ability of generator, and all images generated by generator is correctly judged by discriminator. The loss value and difference value of SSDC generator and discriminator remain near the consistent value, which indicates that the SSDC generator's image feature extraction ability has been strengthened in training.

3.3. *Loss Function*

3.3.1. *Pixel-wise Loss*

We employ the L1 loss function to estimate the pixel loss between the prediction and the target image. The loss function evaluates the class prediction of each pixel vector separately, then averages all pixels. Pixel-wise loss is utilized to estimate image differences in detail, and actively fed back to the network for regulation.

$$L_1 = \sum_{i=1}^{N} \| G(I_i) - J_i \|_1 \tag{8}$$

Where I_i denotes the input hazy image, taking the output of generator $G(I_i)$ and ground truth J_i into estimation. N denotes the total sample in dataset images. It measures the distortion and fidelity between the ground truth image and the dehazed images.

3.3.2. *Perceptual Loss*

Perceptual loss compares the feature obtained by convolution of the real images with the feature obtained by the convolution of the generated picture, so that high-level information, such as the content of the images, is close to the global structure. Perceptual loss will improve the similarity of the entire image frame, and adjust the images information through functions in general.

$$L_P = \frac{1}{CHW} \sum_{c=1}^{C} \sum_{h=1}^{H} \sum_{w=1}^{W} | \varphi_{c,h,w}(I_d) - \varphi_{c,h,w}(I_g) | \tag{9}$$

The symbol φ represents the feature extracted from the pre-trained VGG16[27] model. C, W and H denotes the height, width, and image channel of the feature map in the j-th layer of the backbone network, where I_d denotes dehazed image and ground truth image is I_g.

3.3.3. *Adversarial Loss*

We employ the adversarial loss of GAN. The generator is initialized to convert the hazy image into a haze-free image, and discriminator is employed to distinguish whether the image is real or fake. GAN is trained through a straightforward formula in equation (10), which can be expressed as:

$$L_A = \frac{1}{N} \sum_{i=1}^{N} \log(1 - D(I_i, \tilde{J}_i)) \tag{10}$$

Adversarial loss is a distance measure of each layer in the GAN. Where the J_i denotes the processed output of generator, and I_i is the ground truth image. Optimizer rectify the training direction after estimation.

3.3.4. *Integral Loss Function*

We combine Pixel-wise loss, which is used to make the dehazing image closer to the ground truth, perceptual loss that perfects the balance between the advanced information

of images, adversarial loss is employed to advance restore photo-realistic images, and set weights for each one to adjust parameters dynamically. The parameters are *α1*, *α2* and *α3*.

$$L_T = \alpha_1 L_1 + \alpha_2 L_P + \alpha_3 L_A \tag{11}$$

4. Experiment

We make a quantitatively and qualitatively evaluation, compared to existing methods on various real-world hazy images.

4.1. *Datasets*

Recently, there are various algorithms for image dehazing, whereas, since pair real-world haze maps and haze-free images are laborious to collect on a massive scale for network training, most of the existent datasets for dehazing are artificially synthesized, such as, RESIDE[28], NYU[29], Haze-RD[30], KITTI[31], and Artificial haze, such as D-HAZY[32], O-HAZE[33] and I-HAZE[34]. Datasets can be divided into different categories from indoor, outdoor, haze density and synthesized or not, there are real world haze maps dataset BeDDE[35] as well.

4.2. *Implementation*

Weight parameters *α1*, *α2* and *α3* are set to 1, 0.5 and 0.1, the most critical pixel-level loss parameter is 1, visual loss whose importance is lower than the former determines image balance, and adversarial loss in GAN set to 0.1 as a rule of thumb. Due to the limitations of the experimental facility memory and the large model of some previous method, this type of methods cannot process original size image.

We select appropriate images from the dataset and resize them to 1600×1200×3. 7 of the 45 images in the O-HAZE dataset are randomly selected as the testset, while 5 of 25 pieces in the I-HAZE dataset were selected as test sets. The remaining images are employed as the training set. Each image is divided into 16 pieces with the size of 400*300 to enlarge the trainset. We employ Adam optimizer with initial learning rate of 1-e4 for both generator and discriminator, the whole training epoch is 3,000 times, on the framework Pytorch with a Nvidia TITAN GPU.

4.3. *Metric*

Some quantitative measurement methods are employed to automatically evaluate the image quality objectively, so as to acquire the parameters reflecting the quality on the degree of loss as the evaluation result.

Utilizing images in the same scene on sunny days as the evaluation reference is the ideal objective metric, and estimating the degree of distortion between the dehazing result and the references.

PSNR (Peak Signal to Noise Ratio) is employed to measure the ratio between the maximum possible value of the signal and the distortion noise power that affects the

quality of signal. PSNR is based on the error between the corresponding pixels, and the most widely used objective image evaluation metric.

SSIM[36] (Structural Similarity) is the realization of the structural similarity theory, the structural similarity index defines structural information from the perspective of image composition as being independent of brightness and contrast, reflecting the properties of the object structure in the scene, and modeling distortion into three aspects: brightness, contrast and structure.

LPIPS[37] (Learned Perceptual Image Patch Similarity) permits the features extracted from the network structure of the model can be measured to obtain judgments that are more consistent with human perception. Feature difference between the real sample and the generated sample in the model has been analyzed along with the difference estimated in each channel by L2. Ultimately, LPIPS makes a weight summation for all channels.

4.4. *Result Evaluation*

We draw a comparison (Fig. 6) (Table. 1) between SSDC-GAN and mainstream methods on the dataset O-HAZE since it matches the features of real-world hazy maps. We employ an improved DCP method, which remains haze portion and color deviation at the junction of the sky and objects. In view of too many comparison methods are employed, paper demonstrates the evaluation metrics for DehazeNet and AOD-Net merely. EPDN[38] employs GAN framework and utilizes image translation for images processing, which shows an average increase of 16% in all metrics, but visual contrast reduced and the images towards darker. GCANet[39] has color deviation in dehazed images and FFA-Net remains extensive haze on the whole image. DMPHN[40] is mainly utilized for nonhomogeneous haze images, which brings 6% and 15% improvement on PSNR and LPIPS compared with the first three methods, but SSIM has reduced, meanwhile, DMPHN gets haze residues at the junction of objects with predominant haze has been removed. MSBDN adopts the U-net[41] and appends the SOS module enhancement strategy into decoder for haze removal. Table. 1 shows that MSBDN's dehazing records are higher than the previous algorithm in two metrics, but there is low image cleanliness, residual haze and color deviation.

Fig. 6 and Table. 1 demonstrate the dehazing results of various methods on the O-HAZE dataset, the conclusions are roughly similar to the above. AOD-Net, EPDN, DMPHN and FFA-Net have top numerical performance. Conversely, AOD-Net and FFA-Net retain large area of haze on the images, EPDN tends to be dark with color deviation, while DMPHN is too bright and appends invalid information to the image space.

Alternatively, the dehazed results generated by our algorithm in Fig. 4 and Table. 1, we observe the model with same size connection gets result closer to GT images due to the preservation of the image color information and more visually faithful to the ground-truth. Although SSDC-GAN improves PSNR by 0.15% only, it improves by 38% on LPIPS compare to the second algorithm on O-HAZE, which means that we have reduced the feature difference between real and generated samples in the images. For I-HAZE, Fig. 7 and Table. 2 demonstrate SSDC-GAN achieves the effect closest to GT in

O-HAZE

(a)Hazy (b)DCP (c)EPDN (d)GCANet (e)FFA-Net (f)DMPHN (f)MSBDN (g)Our model (h)GT

Fig. 6. Comparison of the different methods on O-HAZE dataset.

Table 1. Quantitative comparisons with different methods on public datasets O-HAZE.

Methods\Metric	PSNR	SSIM	LPIPS	Runtime
DCP	15.9665	0.6496	0.384	28.68
DehazeNet	15.5421	0.6938	0.328	16.46
AOD-Net	15.6184	0.6374	0.363	3.98
EPDN	18.3350	0.7405	0.301	3.02
GCANet	18.5462	0.7456	0.292	5.84
DMPHN	19.7813	0.7171	0.273	1.34
FFA-Net	18.8655	0.7492	0.316	6.77
MSBDN	20.0987	0.7465	0.254	1.64
SSDC-GAN	20.1304	0.7387	0.184	4.47
GT	+∞	1.00	0.00	×

I-HAZE

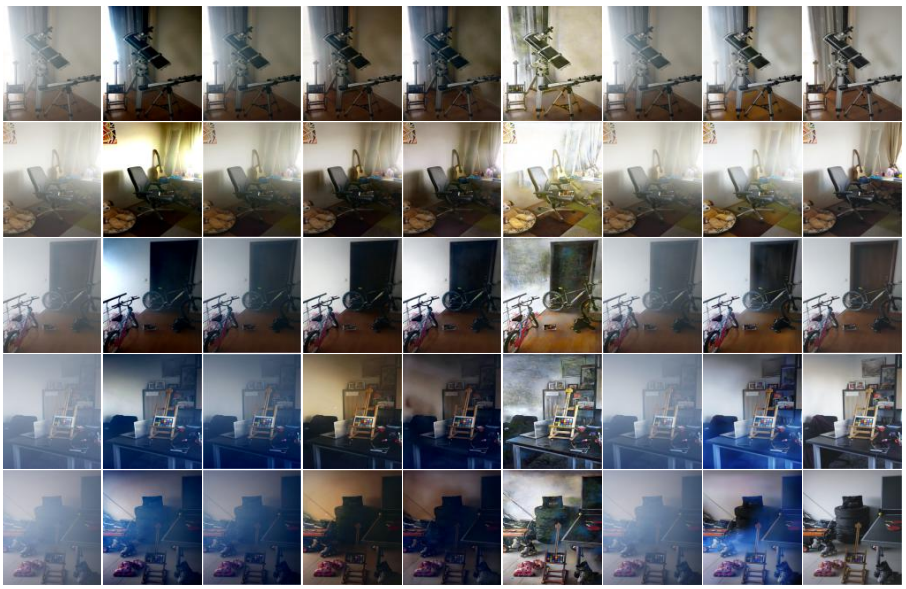

(a)Hazy (b)DCP (c)AOD-Net (d)EPDN (e)GCA-Net(f)DMPHN(f)FFA-Net(g)Our model (h)GT

Fig. 7. Comparison of the different methods on I-HAZE dataset.

Table 2. Quantitative comparisons with different methods on public datasets I-HAZE.

Methods\Metric	**PSNR↑**	**SSIM↑**	**LPIPS↓**
DCP	14.5188	0.7088	0.3044
AOD-Net	16.4720	0.7982	0.2818
EPDN	15.4007	0.7367	0.2956
GCANet	13.5035	0.6727	0.3032
DMPHN	16.4720	0.7642	0.3478
FFA-Net	16.8792	0.8124	0.2678
SSDC-GAN	**18.5607**	**0.8371**	**0.2318**
GT	+∞	1.00	0.00

subjective perception, and the highest index result in metrics. During training processing, the original size dataset images cannot run on the device since excessive memory requirements, and our lightweight model is capable of handling larger size images and achieving superior performance.

4.5. *Ablation Experiments*

To demonstrate the effectiveness and superiority of the connection principle, we conduct experiments under minor quantity of training epochs to evade other factors' affecting. Experimental results compare the performance of the two connected structures:

(a) Hazy;
(b) Ordinary connection model training for 1000 epochs;
(c) Same size dense connection model training for 1000 epochs;
(d) Ground truth.

The results, analyzed through the whole information (Fig. 8, Table. 3) and the details (Fig. 9), demonstrate that the network dehazing effect after employing the same size dense connection bring improvement of 0.88% PSNR and 5.76% LPIPS increase in numerical metrics, which is more consistent with the physical model, visually.

(a) (b) (c) (d)

Fig. 8. Processed images through different connection structures.

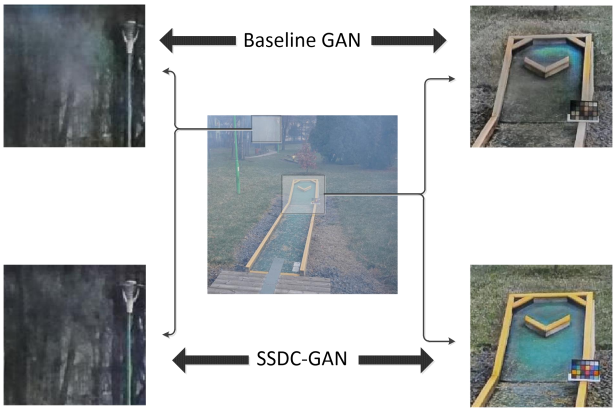

Fig. 9. The effect of connection method on image color saturation and object information recovery.

Table 3. Quantitative comparisons with different methods on public datasets.

	Situation(b)	Situation(c)	Situation(d)
PSNR	22.64	22.84	∞
SSIM	0.77	0.77	1
LPIPS	0.312	0.295	0.000

4.6. *Image Detail Comparison*

We analyze the dehazing effect of multiple methods on object details in the same image, including color and contour information (Fig. 10). Images processed by AOD and EPDN, the overall color towards obscure, especially in the corresponding red box, while, the edge information of trees in the background has confused. DCP and DehazeNet are incapable of dealing with part of multi-detail images, and eliminating residual haze. As for GCANet and FFA-Net, methods have not cleaned up the haze at the edge of the branches and the junction of objects. The contrast of processed images has been enhanced through DMPHN, despite with a limited area of haze on the lawn, and branches too, accompanied by color distortion. Our method generate more visually faithful images to the ground-truth results and images with sharper textures and better color fidelity. Whereas, the remaining haze on the branches may be caused by the small number of iterations.

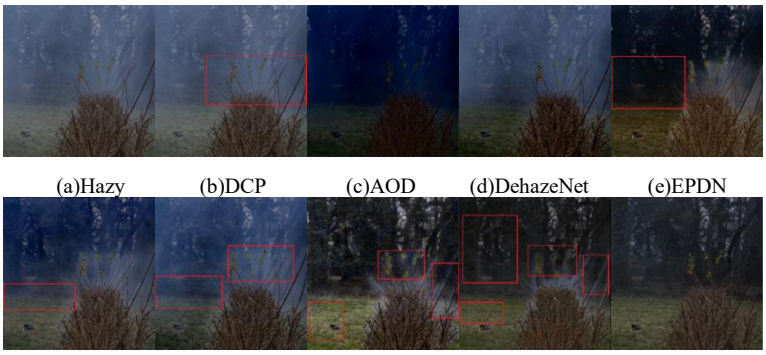

(a)Hazy (b)DCP (c)AOD (d)DehazeNet (e)EPDN

(f)GCANet (g)FFA-Net (h) DMPHN (i)Our model (j)Ground Truth

Fig. 10. Various dehazing method for complex background hazy images and object details. AOD is generally dark, DehazeNet and DCP are similar. There are no red check boxes in the above images.

5. Conclusion

In this paper, we propose a dense connection method that transfers the image information from the encoder to the decoder to preserve the object details and color information of the dehazed images. Simultaneously, a depth discriminator is employed to balance the complexity between the generator and the discriminator, so as to maintain the steadiness in the training and restrain the mode collapse and vanishing gradient.

Various state-of-the-art methods recently have been employed for comparison, and SSDC-GAN performs superior results compare to other approaches. To prove the superiority of the connection principle, we conduct a ablation experiment and demonstrate the two networks differ in their ability to recover image information under small amount training epochs. Nevertheless, SSDC-GAN preserves unnecessary information at times. In the follow-up work, effectual attention mechanism will be applied to focus on retaining fundamental image information and eliminating unnecessary information.

6. Acknowledgements

National Natural Science Foundation of China (Grant/Award Number: 62006073).
Research on Key Technologies of Safe and Efficient Operation of Smart Grid Distribution System (Grant/Award Number: 2019ZYYD020)

References

[1] Middleton, W.E.K.:Vision Through the Atmosphere, Toronto: University of Toronto Press, 2019.
[2] J. T. Chen, B. W. Lei, Q. Y. Song, H. C. Ying, D. Z. Chen and J. Wu, A Hierarchical Graph Network for 3D Object Detection on Point Cloud. *Proceedings of the IEEE/CVF Conference on Computer Vision and Pattern Recognition (CVPR)*, pp. 392-401.
[3] M. S. Ye, S. J. Xu and T. Y. Cao, HVNet: Hybrid Voxel Network for LiDAR Based 3D Object Detection. *Proceedings of the IEEE/CVF Conference on Computer Vision and Pattern Recognition (CVPR)*, pp. 1631-1640.
[4] D. Zoran, M. Chrzanowski, P. S. Huang, S. Gowal, A. Mott and P. Kohli, Towards Robust Image Classification Using Sequential Attention Models. *Proceedings of the IEEE/CVF Conference on Computer Vision and Pattern Recognition (CVPR)*, pp. 9483-9492.
[5] S. F. Huang, T. R. Hui, S. Liu, G. B. Li, Y. C. Wei, J. Z. Han, L. Q. Liu and B. Li, Referring Image Segmentation via Cross-Modal Progressive Comprehension. *Proceedings of the IEEE/CVF Conference on Computer Vision and Pattern Recognition (CVPR)*, pp. 10488-10497.
[6] H. Zhang and V. M. Patel, Densely Connected Pyramid Dehazing Network. *Proceedings of the IEEE Conference on Computer Vision and Pattern Recognition (CVPR)*, pp. 3194-3203.
[7] B. Cai, X. Xu, K. Jia, C. Qing and D. Tao, DehazeNet: An End-to-End System for Single Image Haze Removal. *IEEE Transactions on Image Processing*, vol. 25, no. 11, pp. 5187-5198.
[8] B. Y. Li, X. L. Peng, Z. Y. Wang, J. Z. Xu and D. Feng, AOD-Net: All-In-One Dehazing Network, *Proceedings of the IEEE International Conference on Computer Vision (ICCV)*, pp. 4770-4778.
[9] Cromartie R. and Pizer S.M, Edge-affected context for adaptive contrast enhancement. *Information Processing in Medical Imaging, IPMI*.
[10] Land, E. H, The Retinex Theory of Color Vision. *Scientific American*, vol. 237, no. 6, 1977, pp. 108–129.
[11] K. He, J. Sun and X. Tang, Single Image Haze Removal Using Dark Channel Prior. *IEEE Transactions on Pattern Analysis and Machine Intelligence*, vol. 33, no. 12, pp. 2341-2353.
[12] R. T. Tan, Visibility in bad weather from a single image. *IEEE Conference on Computer Vision and Pattern Recognition*, Anchorage, AK, pp. 1-8.
[13] Q. Zhu, J. Mai and L. Shao, A Fast Single Image Haze Removal Algorithm Using Color Attenuation Prior. *IEEE Transactions on Image Processing*, vol. 24, no. 11.
[14] Y. Qu, Y. Chen, J. Huang and Y. Xie, Enhanced pix2pix dehazing network. *In Proceedings of the IEEE Conference on Computer Vision and Pattern Recognition*, pp. 8160–8168.
[15] W. Q. Ren, L. Ma, J. W. Zhang, J. S. Pan, X. C. Cao, W. Liu and M. H. Yang, Gated Fusion Network for Single Image Dehazing. *Proceedings of the IEEE Conference on Computer Vision and Pattern Recognition (CVPR)*, pp. 3253-3261.
[16] S. D. Das and S. Dutta, Fast Deep Multi-Patch Hierarchical Network for Nonhomogeneous Image Dehazing. *Proceedings of the IEEE/CVF Conference on Computer Vision and Pattern Recognition (CVPR)* Workshops, pp. 482-483.
[17] X. Qin, Z. Wang, Y. Bai, X. Xie and H. Jia, FFA-Net: Feature Fusion Attention Network for Single Image Dehazing. *Proceedings of the AAAI Conference on Artificial Intelligence*, 34(07), 11908-11915.

[18] T. Karras, S. Laine and T. Aila, A Style-Based Generator Architecture for Generative Adversarial Networks. *Proceedings of the IEEE/CVF Conference on Computer Vision and Pattern Recognition (CVPR)*, pp. 4401-4410.
[19] X. Yang, Z. Xu and J. Luo,. Towards perceptual image dehazing by physics-based disentanglement and adversarial training. *In Thirty-second AAAI conference on artifificial intelligence*, 2018.
[20] H. Y. Zhu, V. Chanderasekh, L. Y. Li and J. H. Lim, RR-GAN: Single Image Rain Removal Without Paired Information. *AAAI*.
[21] D. Engin, A. Genc and H. K. Ekenel, Cycle-Dehaze: Enhanced CycleGAN for Single Image Dehazing. *Proceedings of the IEEE Conference on Computer Vision and Pattern Recognition (CVPR)* Workshops, pp. 825-833, 2018.
[22] H. Y. Zhu, X. Peng, V. Chanderasekh, L. Y. Li and J. H. Lim, DehazeGAN: When Image Dehazing Meets Differential Programming. *WiSPNET 2020 conference*.
[23] K. He, X. Zhang, S. Ren and J. Sun, Deep residual learning for image recognition. *Proceedings of the IEEE Conference on Computer Vision and Pattern Recognition (CVPR)*.
[24] Q. Deng, Z. L. Huang, C. C. Tsai and C. W. Lin, HardGAN: A Haze-Aware Representation Distillation GAN for Single Image Dehazing. *Springer*, Cham, 2020.
[25] Y. L. Zhang, Y. P. Tian, Y. Kong, B. N. Zhong and Y. Fu, Residual Dense Network for Image Super-Resolution. *Proceedings of the IEEE Conference on Computer Vision and Pattern Recognition (CVPR)*, pp. 2472-2481.
[26] G. Huang, Z. Liu, L. V. D. Maaten and K. Q. Weinberger, Densely Connected Convolutional Networks. *Proceedings of the IEEE Conference on Computer Vision and Pattern Recognition (CVPR)*, pp. 4700-4708.
[27] K. Simonyan and A. Zisserman, Very deep convolutional networks for large-scale image recognition. *In International Conference on Learning Representations (ICLR)*, 2015.
[28] B. Li, W. Ren, D. Fu, D. Tao, D. Feng, W. Zeng and Z. Wang, Benchmarking single-image dehazing and beyond. *IEEE Transactions on Image Processing (TIP)*, 28(1):492– 505, 2019.
[29] N. Silberman, D. Hoiem, P. Kohli and R. Fergus, Indoor segmentation and support inference from rgbd images. *In European Conference on Computer Vision*, 746–760. Springer.
[30] Y. F. Zhang, D. Li and G. Sharma, Hazerd: an outdoor scene dataset and benchmark for single image dehazing. *IEEE International Conference on Image Processing (ICIP)*. IEEE, 2017.
[31] A. Gaidon, Q. Wang, Y. Cabon and E. Vig, Virtual Worlds as Proxy for Multi-Object Tracking Analysis. *Proceedings of the IEEE Conference on Computer Vision and Pattern Recognition (CVPR)*, pp. 4340-4349.
[32] C. Ancuti, C. O. Ancuti and C. D. Vleeschouwer, D-HAZY: a dataset to evaluate quantitatively dehazing algorithms. *ICIP*, pages 2226–2230, 2016.
[33] C. O. Ancuti, C. Ancuti R. Timofte and C. D. Vleeschouwer, O-HAZE: A Dehazing Benchmark with Real Hazy and Haze-Free Outdoor Images. *CVPR* Workshops, pp. 754-762, 2018.
[34] C. Ancuti, C. O. Ancuti, R. Timofte and C. D. Vleeschouwer, I-HAZE: A dehazing benchmark with real hazy and haze-free indoor images. *CVPR* Workshops, pp. 620–631.
[35] S. Zhao, L. Zhang, S. Huang, Y. Shen and S. Zhao, Dehazing Evaluation: Real-World Benchmark Datasets, Criteria, and Baselines. *in IEEE Transactions on Image Processing*, vol. 29, pp. 6947-6962.
[36] Z. Wang, A. C. Bovik, H. R. Sheikh and E. P. Simoncelli, Image quality assessment: from error visibility to structural similarity. *in IEEE Transactions on Image Processing*, vol. 13, no. 4, pp. 600-612.
[37] R. Zhang, P. Isola, A. A. Efros, E. Shechtman and O. Wang, The Unreasonable Effectiveness of Deep Features as a Perceptual Metric. *Proceedings of the IEEE Conference on Computer Vision and Pattern Recognition (CVPR)*, pp. 586-595.
[38] Y. Y. Qu, Y. Z. Chen, J. Y. Huang and Y. Xie, Enhanced Pix2pix Dehazing Network. *Proceedings of the IEEE/CVF Conference on Computer Vision and Pattern Recognition (CVPR)*, pp. 8160-8168.

[39] D. Chen, M. M. He and Q. N. Fan, et al., Gated Context Aggregation Network for Image Dehazing and Deraining. *IEEE Winter Conference on Applications of Computer Vision (WACV)*, Waikoloa Village, HI, USA, pp. 1375-1383.
[40] S. D. Das and S. Dutta, Fast Deep Multi-Patch Hierarchical Network for Nonhomogeneous Image Dehazing. *Proceedings of the IEEE/CVF Conference on Computer Vision and Pattern Recognition (CVPR)* Workshops, pp. 482-483.
[41] Ronneberger O., Fischer P., Brox T, U-Net: Convolutional Networks for Biomedical Image Segmentation. *Medical Image Computing and Computer-Assisted Intervention – MICCAI.* 2015.

Juan Wang received her B.S. degree from Nanyang Normal University in 2007 and M.S. degree from Xihua University in 2010. and her PhD from Tianjin University in 2015. She is currently a faculty member at Hubei University of Technology. Her research interests include image processing, pattern recognition, and computer vision.

Chang Ding received his B.S.degrees in Jingchu University of Technology, Jingmen, China, in 2019. He is currently pursuing his master's degree at Hubei University of Technology, Wuhan, China. His current research interests are mainly focused on deep learning and image enhancement.

Minghu Wu received his B.S. degree from Communication University of China in 1998 and M.S. degree from Huazhong University of Science and Technology in 2003. and his PhD from Nanjing University of Posts and Telecommunications in 2013. His research interests include artificial intelligence and image processing.

Guanhai Chen received his B.S.degrees in Hubei Polytechnic University, Huangshi, China, in 2021. He is currently pursuing his master's degree at Hubei University of Technology, Wuhan, China. His research interests are image enhancement.

Liquan Guo He is currently pursuing his master's degree at Hubei University of Technology, Wuhan, China. His research interests is Data Augmentation.

Zishan Liu She is currently pursuing her master's degree at Hubei University of Technology, Wuhan, China. Her research interests is object detection.